# Normal-state Ettingshausen, Seebeck, and Hall effects in $La_{2-x}Sr_xCuO_4$

T. Plackowski and M. Matusiak
*Institute of Low Temperature and Structure Research, Polish Academy of Sciences, P.O. Box 1410, 50-950 Wrocław, Poland*
(Received 28 April 1999; revised manuscript received 18 June 1999)

The room temperature values of the Ettingshausen ($P_E$), Hall ($R_H$), and Seebeck ($S$) coefficients as well as of the electrical conductivity ($\sigma$) have been measured for a $La_{2-x}Sr_xCuO_4$ high-$T_c$ superconductor ($x=0.03$–$0.35$). It was found that in the whole composition range $P_E$ is of the order of $10^{-7}$ $m^3K/J$, which is characteristic of typical metals. The Ettingshausen coefficient is positive for $x \lesssim 0.07$ and negative for higher Sr content. Both the Hall coefficient and thermopower decrease logarithmically, with increasing $x$, down to $x \approx 0.3$, then $R_H$ changes sign but $S$ remains positive, exhibiting a minimum. A short review of the interpretations of the Ettingshausen effect is presented. The behavior of the measured transport coefficients have been described by a simple tight-binding-like model with a smooth variation of the Fermi surface curvature from positive to negative, which explains the sign change in $R_H$ and the minimum in $S$. The sign inversion of the Ettingshausen coefficient was interpreted as a result of a competition between two processes generating this effect, called ''scattering'' and ''curvature'' mechanisms. [S0163-1829(99)00445-2]

## I. INTRODUCTION

The problem of normal-state transport phenomena in high-$T_c$ (HTC) superconductors remains a central challenge since their discovery. That is because the characteristic dependences on temperature and composition of many transport properties may be regarded as a hallmark of the HTC's, on par with their superconducting properties. For example, in many of the HTC families the thermopower changes sign at optimal carrier concentration.[1] The linearity of resistivity for the optimally doped samples in a wide temperature region is also one of their most well-known features.[2] The Hall coefficient for optimally doped samples varies as $1/T$, which results in the $1/T^2$ dependence of the Hall mobility $\mu_H$. Then it appeared that the $1/T^2$ dependence of $\mu_H$ is more universal. It applies not only to the optimally doped, but also to the underdoped and overdoped materials.[3]

In this work we present the measurements of the Ettingshausen coefficient, one of the less known transport coefficients. Our aim was to complement the present knowledge of the normal state properties of HTC materials, and, hopefully, to search for some new universalities. The Ettingshausen effect is a thermal analog of the Hall effect [the definition and sign convention are shown in Fig. 1(a)]. The difference with respect to the Hall effect lies in the fact that it is the temperature difference that is measured in the direction perpendicular to both the current and field directions, instead of the voltage difference. Measurements of the Ettingshausen effect were supplemented by measurements of the Hall effect and thermoelectric power.

In the present work we have chosen the $La_{2-x}Sr_xCuO_4$ (LSCO) solid solution ($x=0.03$–$0.35$), which exhibits the full range of behavior versus chemical composition that is characteristic of the layered copper-oxide superconductors. The carrier concentration may be controlled by the Sr concentration $x$. One could therefore investigate the doping dependence from the semiconducting region ($x \lesssim 0.05$), through the underdoped ($0.05 \lesssim x \lesssim 0.17$) and overdoped ($0.17 \lesssim x \lesssim 0.30$) regions with superconductivity, up to the heavily doped metallic region with no superconductivity ($x \gtrsim 0.30$).[4] Moreover, LSCO has a simple crystal structure with single $CuO_2$ layers. It has no Cu-O chains as in $YBa_2Cu_3O_{7-\delta}$ nor complicated modulation of the separating and spacing layers as in Bi- and Tl-based materials. The LSCO is also attractive for our purpose due to a change of the sign of the Hall effect, which some authors observed at the Sr concentration $x \approx 0.30$.[5,6] For all samples we have measured the room-temperature values of the Ettingshausen and Hall effects as well as of the thermoelectric power. The samples were also characterized by the x-ray and electrical resistivity measurements.

## II. MODELS OF THE ETTINGSHAUSEN EFFECT

### A. Definitions and thermodynamic relations between transversal magnetothermal coefficients

The Hall and Ettingshausen effects are two of the four transversal magnetothermal effects:

$$\nabla\Phi_\perp = R_H \ \vec{j}\times\vec{B}, \quad \text{the Hall effect,} \tag{1}$$

$$\nabla T_\perp = P_E \ \vec{j}\times\vec{B}, \quad \text{the Ettingshausen effect,} \tag{2}$$

$$\nabla\Phi_\perp = Q_N \ \nabla T\times\vec{B}, \quad \text{the Nernst effect,} \tag{3}$$

$$\nabla T_\perp = S_{RL} \ \nabla T\times\vec{B}, \quad \text{the Righi-Leduc effect,} \tag{4}$$

where $R_H$, $P_E$, $Q_N$, $S_{RL}$ are the respective coefficients, $\nabla\Phi_\perp$ and $\nabla T_\perp$ are the transversal gradients of electrical potential and temperature, respectively, caused by the presence of magnetic field ($\vec{B}$) perpendicular to the electrical current ($\vec{j}$) or heat flux ($\vec{q}\sim\nabla T$). All these coefficients are interconnected by three fundamental relations that were considered by Bridgman[7] in terms of thermodynamics of reversible processes:

 

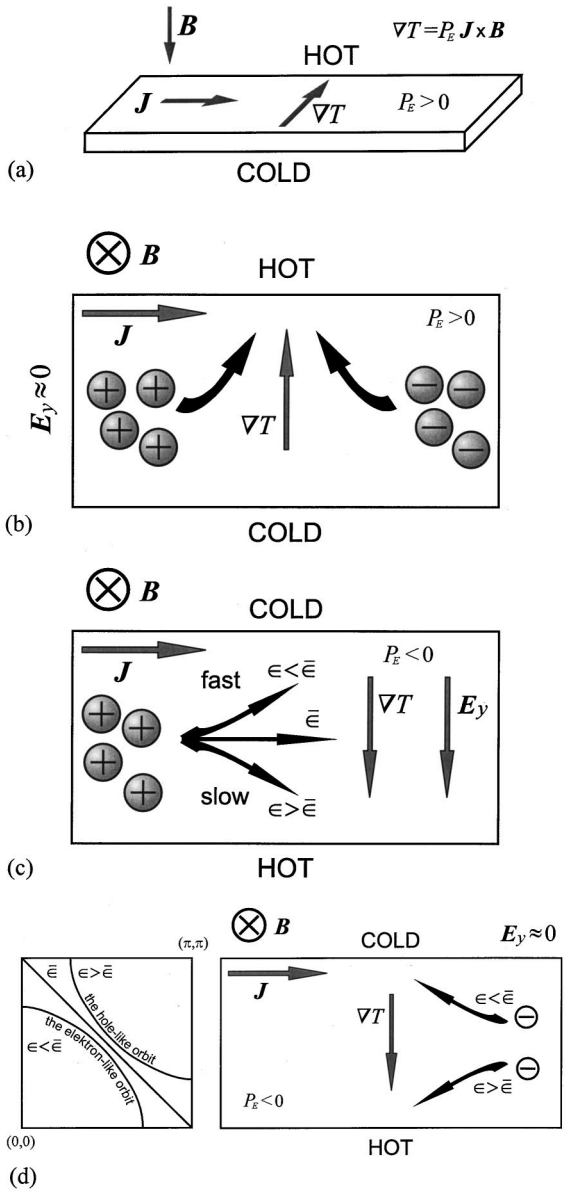


FIG. 1. (a) The sign convention for a positive Ettingshausen effect; (b) the mechanism of the Ettingshausen effect in semiconductors; (c) the Ettingshausen effect in metals in the nearly free electrons picture—the ''scattering'' mechanism (black arrows denote drift direction); (d) the Ettingshausen effect in metals in the case of the zero curvature of the Fermi surface—the ''curvature'' mechanism (black arrows denote movement directions). The left panel shows different types of the Fermi surfaces enclosed by the distribution of the electrons energies ($P_E$, the Ettingshausen coefficient; $B$, the magnetic field; $E$, the electric field; $J$, the electrical current; $\nabla T$, the temperature gradient; $\epsilon$, the energy).

$$P_E=\frac{T\mu_T}{\kappa\rho}R_H, \tag{5}$$

$$Q_N=\frac{\mu_T}{\rho}R_H, \tag{6}$$

$$S_{RL}=\frac{1}{\rho}R_H, \tag{7}$$

where $\kappa$ is the total thermal conductivity and $\mu_T$ is the Thomson coefficient. The above relations are presented in the form expressing all the coefficients in terms of the Hall coefficient. As indicated in (Ref. 8), the coefficients from pairs ($R_H$, $S_{RL}$) and ($P_E$, $Q_N$) should be necessarily of the same sign, whereas the sign relation between pairs is not strictly determined and depends on the sign of the Thomson coefficient. In case the thermal conductivity is dominated by the electronic contribution ($\kappa\approx\kappa_e$) and supposing the validity of the Wiedemann-Franz law, the first of the above relations may be simplified to

$$P_E=\frac{\mu_T}{L_0}R_H, \tag{8}$$

where $L_0$ is the Lorentz number.

### B. Semiconductors

The Ettingshausen effect has a simple, intuitive explanation within the relaxation-time approximation for both semiconductors and metals, however two different physical mechanisms are dominating in these materials. As considered by Paranjape and Levinger,[9] in case of semiconductors the Ettingshausen effect may be especially large in materials in which two type of charge carriers with opposite signs are present, e.g., in intrinsic semiconductors [see Fig. 1(b)]. Forced by the electric field $E_x$ electrons and holes move in opposite directions, but in the presence of magnetic field $B_z$ perpendicular to current direction they will turn toward the same side of the sample. Hence, on this side the density of the hole-electron pairs will increase above the thermal equilibrium value, whereas on the opposite side of the sample this density will be decreased. Thus, on the side with elevated pairs density the processes of pairs recombination will prevail over the creation processes. Therefore, the energy released in recombination acts will make this side hotter. Analogically, the opposite side will be made colder due to domination of creation processes, thus resulting in the lateral temperature gradient $\nabla_y T$.

The approximate formula for the Ettingshausen effect in semiconductors obtained within the above picture is the following:[9]

$$P_E=\frac{E_g}{\kappa e}\frac{n_e\mu_e n_h\mu_h}{(n_e\mu_e+n_h\mu_h)^2}(\mu_e+\mu_h), \tag{9}$$

where gap energy $E_g$ is the difference between mean energy of electrons $E_c$ and mean energy of holes $E_v$ (this is the energy released in each act of the hole-electron recombination), $\kappa$ is the total thermal conductivity, $e$ is the elementary charge, and $n_e$, $\mu_e$, $n_h$, and $\mu_h$ denote carrier densities and mobilities of the electrons and holes, respectively. It should be underlined that here that the carrier densities do not include the carrier signs and by the assumed convention $e>0$. Thus, the Ettingshausen coefficient for semiconductors is always positive, irrespective of whether the dominant carriers are electrons or holes. The Hall coefficient within the same two-band model is given by

$$R_H=\frac{(n_e\mu_e^2-n_h\mu_h^2)}{(n_e\mu_e+n_h\mu_h)\sigma}, \tag{10}$$

where $\sigma$ denotes the total electrical conductivity. Comparing the formulas for $P_E$ and $R_H$ a next conclusion may be formulated, that the Ettingshausen coefficient for semiconductors is the highest when the Hall coefficient is close to zero, i.e., when the contributions to the electrical conductivity by electrons and holes are comparable. As seen from the formula (9), the value of the Ettingshausen effect for semiconductors is governed by gap width $E_g$ and by the thermal conductivity (for semiconductors $\kappa$ is usually dominated by the phonon contribution). Typical measured values of the Ettingshausen coefficients for semiconductors are positive, indeed, and of the order $10^{-2}$–$10^{-4}$ $m^3K/J$ [Ge (Ref. 10); Si (Ref. 11); PbSe, PbTe (Ref. 12)].

### C. Metals—nearly-free electrons model

As shown by Fieber, Nedoluha, and Koch (FNK),[8] the Ettingshausen effect in metals has a quite different origin and its magnitude is governed by different material parameters. Physically, in the nearly-free electron (NFE) picture the transversal temperature gradient within a metal sample is caused by the dependence of the mean time between collisions $\tau$ of the charge carriers on their energy[9] [an example for nearly-free holes is shown in Fig. 1(c)]. The $\tau$ determines the mean drift velocity $v$ of the carrier with the particular energy $\epsilon$:

$$\vec{v}(\epsilon)=\vec{E}\mu(\epsilon)=\vec{E}e\tau(\epsilon)/m, \tag{11}$$

where $e$ and $m$ are the electron charge and mass, respectively. In the magnetic field each moving carrier is subjected to the Lorenz force where the value is also dependent on the carrier velocity,

$$\vec{F}(\epsilon)=e\vec{v}(\epsilon)\times\vec{B}. \tag{12}$$

In the steady state there is no electrical current in the $y$ direction since the Hall voltage $E_y$ is developing compensating the Lorenz force. However, the compensation is exact only for some intermediate energy $\overline{\epsilon}$ ($\overline{\epsilon}\approx E_F$), or for some intermediate drift velocity $v_x(\overline{\epsilon})$,

$$ev_x(\overline{\epsilon})B_z=-eE_y. \tag{13}$$

The carriers with energy $\epsilon>\overline{\epsilon}$ will tend to turn to one side of the sample (hot side), whereas the carriers with $\epsilon<\overline{\epsilon}$ will turn to the other side of the sample (cold side), thus resulting in a transversal temperature gradient $\nabla T_y$. Though in general, $\tau(\epsilon)$ and thus the drift velocity $v(\epsilon)$ may be either increasing or decreasing the function of energy, so the carriers with, e.g., $\epsilon>\overline{\epsilon}$ may be deflected to any side, depending on the slope of the $\tau(\epsilon)$ dependence.

This pictorial model of the Ettingshausen effect in metals was described by a formula derived in Ref. 8 for a parabolic band,

$$P_E=\frac{T}{n_H}\left(\frac{\partial\ln[\tau(\epsilon)]}{\partial\epsilon}\right)_{\epsilon=\zeta}=eR_HT\left(\frac{\partial\ln[\tau(\epsilon)]}{\partial\epsilon}\right)_{\epsilon=\zeta}, \tag{14}$$

where $\zeta$ is the chemical potential and $n_H$ is the carrier density determined by the Hall effect. We would like to emphasize that now $n_H$ includes the charge sign. As seen, the sign of the Ettingshausen effect for metals is a product of the signs of the Hall coefficient and of the $\partial\tau(\epsilon)/\partial\epsilon$ derivative at the Fermi surface. Since for the parabolic band $\mu_T\sim T(\partial\ln\tau)/\partial\epsilon$,[8] we again obtain the relation between $P_E$ and $R_H$ in the form derived by Bridgman (see Eqs. 5 and 8).

In analogy to the considerations for the thermopower from Ref. 13 two simple cases may be regarded. At low temperatures ($T\ll\Theta_D$, where $\Theta_D$ is the Debye temperature) we could deal with nearly-free electrons scattered from nonmagnetic impurities. Provided that mean-free path $l$ is energy independent, one could obtain that $\tau(\epsilon)\sim\epsilon^{-1/2}$ (Ref. 14) and thus $d\tau/d\epsilon<0$. This could be intuitively explained in the following way: the high-energy carriers are stronger scattered and, for this reason, they have lower drift velocity. Therefore, in that case the Ettingshausen effect will have an opposite sign to the Hall effect. As shown in Refs. 8 and 15 in this approximation the formula (14) for the Ettingshausen effect in metals may be simplified to the form

$$P_E=-\frac{T}{2n_HE_F}=-\frac{eTR_H}{2E_F}, \tag{15}$$

where $E_F$ is the Fermi energy and $n_H$ is positive for holes.

The second case refers to high temperature ($T>\Theta_D$). Assuming elastic electron-phonon scattering one obtains $\tau(\epsilon)\sim\epsilon^{3/2}$ and $d\tau/d\epsilon>0$. The Ettingshausen coefficient may in that case be expressed as

$$P_E=\frac{3T}{2n_HE_F}=\frac{3eTR_H}{2E_F}. \tag{16}$$

As seen, if the parabolic band can be assumed then at sufficiently high temperature the Ettingshausen and Hall coefficient would have identical signs.

Typical values of the Ettingshausen coefficients for metals are much lower then for the semiconductors and are of the order $10^{-7}$–$10^{-8}$ $m^3K/J$. A negative Ettingshausen coefficient was observed for Ag, Cd, Cu, Fe, Zn, and Au, whereas it was positive for Al, Co, and Ni. The Ettingshausen effect and the Hall effect have opposite signs for Al, Cd, Fe, Ni, and Zn, whereas the same signs for Ag, Co, Cu, and Au.[7,16] The Ettingshausen coefficient is much higher for semimetals [$\sim10^{-4}$ $m^3K/J$ for Sb and $\sim10^{-3}$ $m^3K/J$ for Bi (Ref. 7)] and for rare earths [$\sim10^{-3}$ $m^3K/J$ for Y, Gd, Tb, and Dy (Ref. 17)].

### D. Metals—general model

If the parabolic band cannot be assumed then the formula for the Ettingshausen effect in metals should be used in its more general form derived in[8]

$$P_E=-\frac{T}{n_{eff}\tau}[\tau f_k]'_{\epsilon=\zeta}, \tag{17}$$

where $n_{eff}$ is the effective density of free electrons ($n_{eff}$ includes the electron charge sign, i.e., $n_{eff}<0$). The function $f_k$ (by FNK called as ''Freiheitszahl''—the freedom number) is defined by a modified acceleration equation,[18]

$$\frac{d\vec{v}_g}{dt}=\frac{\vec{F}}{m_e}f_k, \tag{18}$$

where $\vec{v}_g=1/\hbar\nabla_k E$ is the group velocity of electron, $\vec{F}$ is the force, and $m_e$ is the free-electron mass. In general, $f_k$ is a tensor,

$$f_{ij}=m_e\left(\frac{1}{m_{eff}}\right)_{ij}=\frac{m_e}{\hbar^2}\frac{\partial^2 E}{\partial k_i \partial k_j},$$

where $m_{eff}$ is the effective mass. After transformation to the main axes the average value of $f_k$ may be expressed by [for a two-dimensional (2D) case applicable for HTC superconductors],

$$f_k(k_x,k_y)=\frac{m_e}{2\hbar^2}\left(\frac{\partial^2 E}{\partial k_x^2}+\frac{\partial^2 E}{\partial k_y^2}\right). \tag{19}$$

The function $f_k=\text{const}>0$ for case of nearly-free electrons (the bottom of the band) and $f_k=\text{const}<0$ for nearly-free holes (the top). In order to use it for calculations of transport coefficients, $f_k$ should be averaged over the Fermi surface. This can be done in analogy to the standard considerations for the Hall coefficient,[19] using the group velocity $v_g$ as a weighting function:

$$\hat{f}_k=\frac{\int f_k v_g d\mathbf{S}}{\int v_g d\mathbf{S}}. \tag{20}$$

The integrations go over the Fermi surface. Now, both $\hat{f}_k$ and $n_{eff}$ can be expressed in terms of elements of the conductivity tensor;

$$\hat{f}_k(\epsilon)=-\frac{m_e}{|e|\tau}\frac{\sigma_{xy}}{\sigma_{yy}}=-\frac{m_e}{2\hbar}\frac{\int v_g^2(1/\rho)d\mathbf{S}}{\int v_g d\mathbf{S}}, \tag{21}$$

$$n_{eff}(\epsilon)=-\frac{m_e}{e^2\tau}\sigma_{xx}=-\frac{m_e}{8\pi^3\hbar}\int v_g d\mathbf{S}, \tag{22}$$

where $1/\rho$ denotes the Fermi surface curvature ($\rho$ is the radius of the Fermi surface). The above formula was derived under the assumption that the relaxation time $\tau$ depends only on energy: $\tau=\tau(\epsilon)$. The case of low-field limit ($\omega_c\tau\ll 1$, $\omega_c$ is the cyclotron frequency) is also assumed. The conductivities $\sigma_{ij}$ are expressed by standard formulas[19] (here adapted for the 2D case and square symmetry):

$$\sigma_{xx}=\sigma_{yy}=\frac{e^2\tau}{8\pi^3\hbar}\int v_g d\mathbf{S}, \tag{23}$$

$$\sigma_{xy}=\frac{e^3\tau^2}{4\pi^3\hbar^2}\int v_g^2(1/\rho)d\mathbf{S}. \tag{24}$$

We would like to underline that the assumption of the 2D case allows us to treat the Fermi surface curvature at a certain point as a single number. In the 3D case the curvature should be described by two numbers.

Physically, $\hat{f}_k$ is a measure of the average curvature of the Fermi surface. It is easily understandable, if the Hall coefficient $R_H$ is expressed in terms of the $\hat{f}_k$ function,[8]

$$R_H=\frac{\sigma_{xy}}{\sigma_{xx}\sigma_{yy}}=\left(\frac{\hat{f}_k}{|e|n_{eff}}\right)_{\epsilon=\zeta}, \tag{25}$$

where $n_{eff}$ includes the electron sign, as in Eq. (17). Near the band edges, in the NFE approximation, $\hat{f}_k\approx\text{const}$ and the formula for the Hall coefficient may be simplified to the classical expression

$$R_H\approx\frac{1}{en_H}, \tag{26}$$

where

$$n_H=\hat{f}_k n_{eff}=\frac{m_e}{m_{eff}}n_{eff} \tag{27}$$

is the so-called Hall concentration; the $n_H<0$ for nearly-free electrons (the bottom of the band), $n_H>0$ for nearly-free holes (the top).

The generalized formula for $\hat{f}_k$ allows the calculation of the Ettingshausen coefficient besides the NFE approximation. The formula (17) may be expanded to the form:

$$P_E=-\frac{T}{n_{eff}}\left[\frac{\partial\ln\tau}{\partial\epsilon}\hat{f}_k+\frac{\partial\hat{f}_k}{\partial\epsilon}\right]_{\epsilon=\zeta}. \tag{28}$$

In the NFE case (i.e., near the band edges) $\hat{f}_k$ is constant, the second term in the above formula disappears and it reduces to the formula (14). In the middle of the band $\hat{f}_k$ is energy dependent. However, taking into account that $\hat{f}_k>0$ near the bottom of the band and $\hat{f}_k<0$ near the top, one could expect that $\partial\hat{f}_k/\partial\epsilon<0$ [assuming that the dispersion law $E(k)$ is monotonic between the bottom and top of the band]. Thus, the new contribution to the Ettingshausen effect provided by the second term is always negative, irrespective of the location of the Fermi level within the band. It is worth emphasizing that this contribution is independent of the scattering mechanism.

Physically, both contributions arise from the dispersion of electrons energies around the Fermi energy (the width of this dispersion is proportional to $T$). As explained in the previous subsection, the first term is caused by the fact that electrons of different energy have different $\tau$ and, hence, different drift velocity. In magnetic field this results in deflecting electrons of different energy to different sides of the sample [see Fig. 1(c)]. We will call this the ''scattering'' mechanism. The second term, however, is caused by the fact that in the magnetic field electrons of different energy are moving along isoenergetic surfaces of different average curvature. Thus, their trajectories are differently influenced by the magnetic field. We will call this the ''curvature'' mechanism. This mechanism is dominating in the case when $\hat{f}_k\approx 0$ (i.e., $R_H\approx 0$) or, in other words, for the Fermi surface of nearly zero average curvature [see Fig. 1(d)]. In this case the first, ''scat-

tering'' term in formula (28) disappears. Since $R_H \approx 0$, no transversal voltage develops between sides of the sample ($E_y \approx 0$). The electrons of some intermediate energy $\bar{\epsilon}$ ($\bar{\epsilon} \approx E_F$), i.e., moving along the isoenergetic surface with zero-average curvature, will not be deflected by the magnetic field. However, the electrons with $\epsilon < \bar{\epsilon}$ and $\epsilon > \bar{\epsilon}$ will move along surfaces of electronlike and holelike curvatures, respectively. Therefore, they will be turned in opposite directions and the transversal temperature gradient will develop. Since the ''hot'' electrons ($\epsilon > \bar{\epsilon}$) are always moving along holelike isoenergetic surfaces then the sign of the Ettingshausen effect will be always negative.

We also would like to stress that in the case described above the Bridgman relation connecting $P_E$ and $R_H$ [Eqs. (5) and (8)] is no more valid (here $P_E \neq 0$, whereas $R_H = 0$). It is not a surprise, since the Thomson coefficient, which is expressed by[8]

$$\mu_T \approx -\frac{\pi^2 k_B^2 T}{3|e|} \frac{[\tau f_k]'_{\epsilon=\zeta}}{\tau f_k}, \tag{29}$$

would exhibit a singularity if $\hat{f}_k \approx 0$ (and, thus, $R_H \approx 0$), but the product $\mu_T R_H$ may have a finite value.

### III. SAMPLES AND EXPERIMENT

Polycrystalline samples of $La_{2-x}Sr_xCuO_4$ were produced following the standard solid-state technique from high-purity $La_2O_3$, $SrCO_3$, and CuO substrates. The powders were mixed and prefired in air at 950 °C for 24 h. After pulverization, the materials were mixed, pressed and sintered at 1000 °C for 60 h. Then they were regrounded, pelletized and, except one sample, refired at 1050 °C for 72 h in air under pressure of 1 bar. Only the sample of $La_{1.65}Sr_{0.35}CuO_4$ was sintered in oxygen under the pressure of 300 bar at 1000 °C for 48 h. All products were confirmed to be single phase by powder x-ray diffraction. The lattice constants at room temperature were plotted against the Sr content in Fig. 2(a), they agree well with the previous reports.[5] The observed systematic change of the lattice parameters upon doping guarantees the well-controlled stoichiometry. The superconducting critical temperatures, determined by electrical resistivity measurements results, are presented in Fig. 2(b). The resistivity curves are shown in Fig. 3.

During the thermopower measurements the samples were clamped between two copper blocks, one of which was kept at a temperature a few degrees higher then the other ($1 < \Delta T < 4$ K). The absolute TEP was obtained relative to the Seebeck coefficient of copper.

The Hall effect was measured by a standard method at the magnetic field of 12 T. The samples have been cut into the shape of slabs of thickness of 0.25–0.35 mm, width of 2.5–3 mm, and length of 9–10 mm. We have been rotating the sample by 180° and reversing the current direction many times to exclude the influence of mismatching of the Hall contacts positions and of detrimental emf's.

The shape of the samples using the Ettingshausen-effect measurements was identical to that used for the Hall-effect investigations. The experimental setup is shown in Fig. 4. Since the weak thermal gradient due to the Ettingshausen effect may be easily overridden by the Joule and Thomson

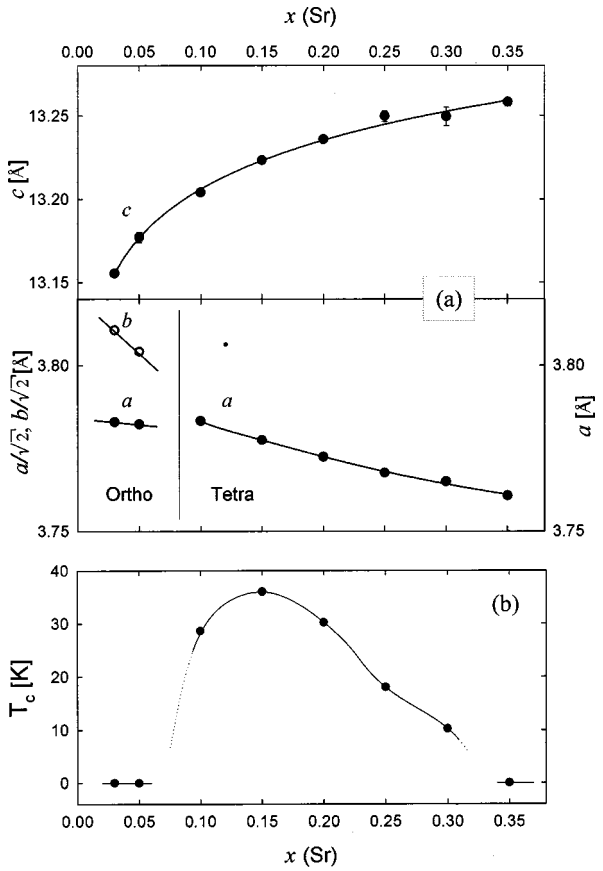


FIG. 2. The lattice parameters (a) and the critical temperatures (b) for $La_{2-x}Sr_xCuO_4$.

effects, special measures have been taken to extract it from the background. The ends of the sample ($A$) were thermally anchored to a large copper block ($C$) through smaller copper blocks ($B$) to carry away the Joule heat. The transversal temperature difference $\Delta T$ has been measured by a differential thermocouple. The temperature of the copper block ($C$) has been measured by a carbon-glass thermometer ($E$). To eliminate the influence of the thermal gradients due to the Joule and Thomson effects the odd symmetry of the Ettingshausen temperature difference with respect with the direction of the magnetic field and electrical current has been

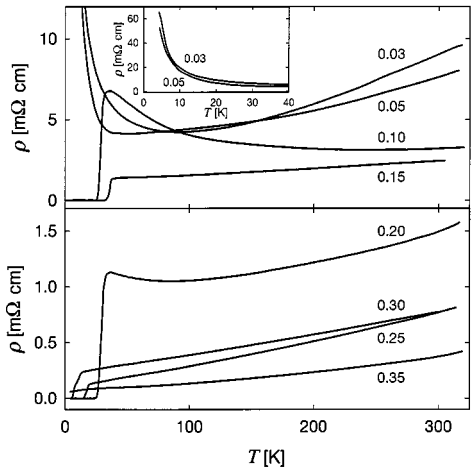


FIG. 3. The electrical resistivity for $La_{2-x}Sr_xCuO_4$.

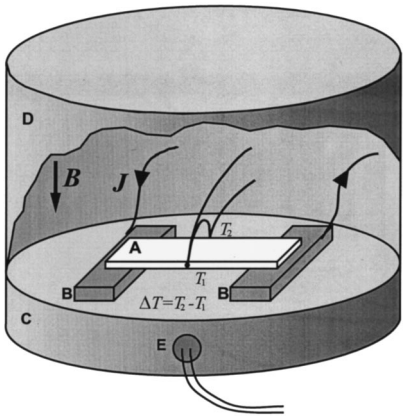


FIG. 4. Experimental setup for the Ettingshausen-effect measurements. See text for details.

exploited. More details regarding the measurements of the Ettingshausen effect have been presented in Ref. 20.

## IV. RESULTS

The samples with $x=0.03$ and 0.05 are nonsuperconducting and exhibit a sudden increase of resistivity for temperatures below $\sim 50$ K (see Fig. 3). The first superconducting sample ($T_c=28.6$ K) with $x=0.10$ is underdoped and reveals semiconductorlike temperature dependence of the resistivity. The sample with $x=0.15$ is closest to the optimal doping—it has the highest $T_c=36.0$ K among all samples. The samples with $x=0.20$, 0.25, and 0.30 are overdoped, their values of $T_c$ are gradually decreasing (30.2, 18.0, and 10.2, respectively) and they reveal a metal-like $\rho(T)$ dependences. The last overdoped sample with $x=0.35$ is nonsuperconducting and it exhibit the lowest resistivity among all the samples.

Figure 5 presents the room-temperature values of the electrical conductivity (a), the thermopower (b), the Hall coefficient (c), and the Ettingshausen coefficient (d) for all samples of $La_{2-x}Sr_xCuO_4$ versus $x$, the Sr concentration. As seen in Fig. 5(a), the values of the room-temperature conductivity increase monotonically as the Sr content $x$ is growing. The room-temperature values of the thermoelectric power $S$ [Fig. 5(b)] are logarithmically decreasing with $x$ down to the value of $x=0.20$. The smallest value of $S$ was observed for $x=0.30$, whereas the sample with $x=0.35$ is breaking the tendency: its value of $S$ is higher than that for the preceding sample with $x=0.30$. All the measured values are positive, thus the whole series of $La_{2-x}Sr_xCuO_4$ clearly distinguishes itself from the majority of HTC superconductors families, whereas for the in-plane TEP a crossover from positive to negative values were observed nearby the optimal doping.[1,21]

Similar to the thermopower, the room-temperature values of the Hall coefficient $R_H$ [Fig. 5(c)] are positive and they are logarithmically decreasing with $x$. The heaviest overdoped sample with $x=0.35$ is also an exception, in contrast to all other samples its $R_H$ value is negative (this is in accordance with observations of other authors[5,6]). However, as shown in the inset, in the linear scale the variation of $R_H$ in the vicinity of the point of the sign inversion may be regarded as smooth and monotonic. It is obvious that there $1/R_H$ cannot be simply used for calculation of either carrier concentration $n$ or the mobility $\mu$. Otherwise, $n$ would diverge to infinity or $\mu$ would approach zero for the Sr concentration where $R_H \approx 0$ ($x \approx 0.32$), in clear contrast to the observed smooth variation of electrical resistivity. Since both

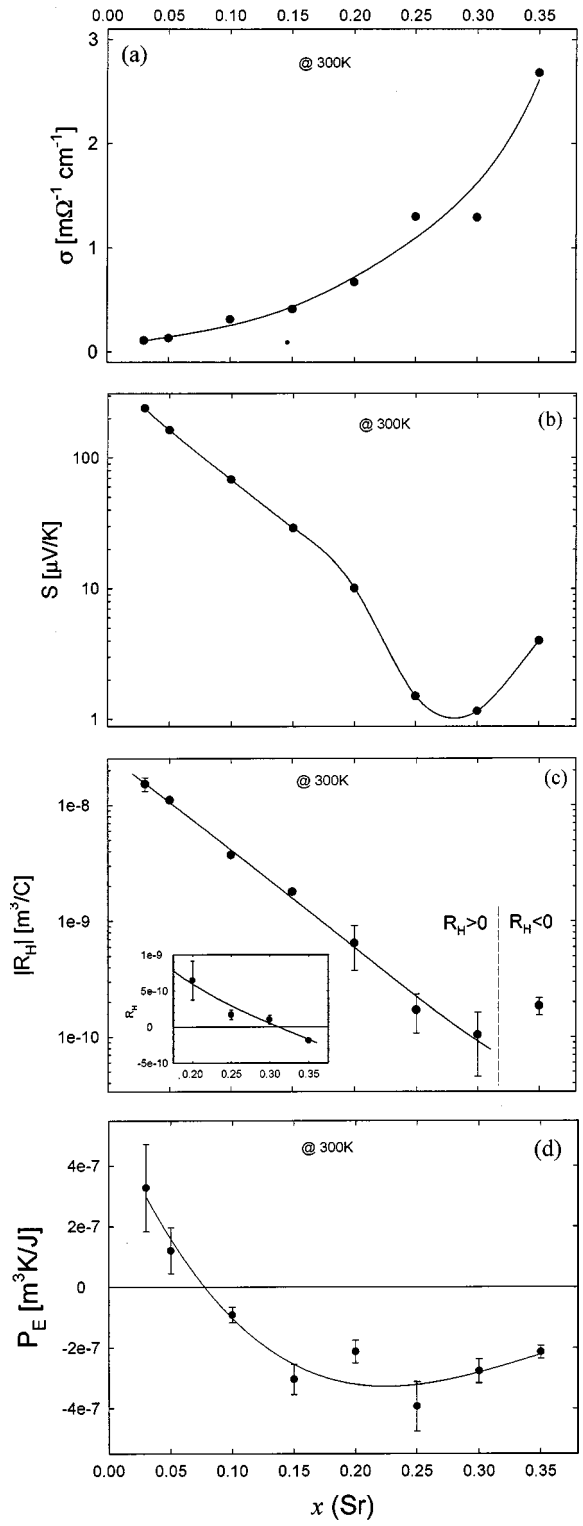


FIG. 5. The room-temperature values of different transport coefficients for a series $La_{2-x}Sr_xCuO_4$ samples ($x=0.03$–0.35): the electrical conductivity (a), the thermoelectric power (b), the Hall coefficient (c), and the Ettingshausen coefficient (d). The inset in panel *c* shows, in the linear scale, the Hall coefficient in the vicinity of the Sr concentration, where $R_H$ changes sign.

$R_H$ and $S$ vary logarithmically with Sr doping, their linear mutual dependence may be expected. It is shown below in Fig. 9(a), where an almost linear dependence over two orders of magnitude, both in $R_H$ and $S$, may be seen.

The values of Ettingshausen coefficient are shown on the last bottom panel [Fig. 5(d)]. The coefficients are positive for the two nonsuperconducting samples with low Sr concentration ($x=0.03$ and 0.05). For all other samples the sign of the Ettingshausen effect is negative and the coefficient values are weakly dependent on Sr content (the crossover Sr concentration may be assessed as $x\approx 0.07$). All the values are of the order of $10^{-7}\mathrm{m}^3\mathrm{K/J}$, which is typical for good metals (see the Introduction), however an important comment should be made to this statement. Namely, it was indicated in numerous papers that far above $T_c$ the total thermal conductivity $\kappa$ of the HTC superconductors is not dominated by the electron contribution $\kappa_e$, as for typical metals. Different evaluations have shown that the ratio $\kappa_e/\kappa$ is usually of the order of $0.01-0.1$ for polycrystalline samples [e.g., for $YBa_2Cu_4O_8$ (Ref. 22), for $RBa_2Cu_3O_7$ (Ref. 23)] and at most of the same order as the phonon contribution ($\kappa_{ph}$) for good quality single crystals [e.g., for $YBa_2Cu_3O_7$ (Ref. 24)], for $Bi_2Sr_2YCu_2O_8$ (Ref. 25)]. The phonon contribution dominates also for the nonsuperconducting but metallic compound of $PrBa_2Cu_4O_8$.[26] Similar observations have been also made for $La_{2-x}Sr_xCuO_4$,[27,28] where $\kappa_e/\kappa\sim 0.01$ have been assessed assuming the applicability of the Wiedemann-Franz law. Thus, for HTC materials in the normal state the actual thermal conductivity is much higher than that expected by FNK model,[8] where only $\kappa_e$ has been taken into consideration. Therefore, if the transversal Ettingshausen temperature gradient is shortened additionally by $\kappa_{ph}$, then the measured $P_E$ values will be considerably suppressed in respect to FNK model predictions. In other words, to be able to compare the experimental results for $P_E$ with the model predictions they should be corrected by the $\kappa/\kappa_e$ factor. One could expect that this factor may be especially pronounced for $La_{2-x}Sr_xCuO_4$ samples with low-Sr concentration.

## V. PHENOMENOLOGICAL MODEL

Figure 6(a) presents the ratio of the number of holes per formula unit evaluated from the Hall coefficient, $n_{f.u.}=1/(2VeR_H)$ (the unit-cell volume $V$ contains two formula units of $La_{2-x}Sr_xCuO_4$) to the Sr content $x$. Since the $La^{+3}$ ions are replaced by $Sr^{+2}$ ions, the Sr content may be regarded as the number of holes added per formula unit due to La/Sr substitution. As seen, $n_{f.u.}$ and $x$ are approximately equal only for low Sr concentration, for $x\lesssim 0.10$ (as already observed in Refs. 5 and 29). For higher $x$ values ($x>0.10$) the charge carrier concentration indicated by the Hall coefficient is significantly higher than $x$. To explain this one has to abandon the nearly-free electron picture and use a more general formula for the Hall coefficient from Eq. (25) taking into account the geometry of the Fermi surface. If one interprets the number of holes introduced by the La/Sr substitution as the effective number of free electrons $n_{eff}$ one could calculate the experimental values [see Fig. 6(b)] of the freedom number $\hat{f}_k$ [see Eq. (27)],

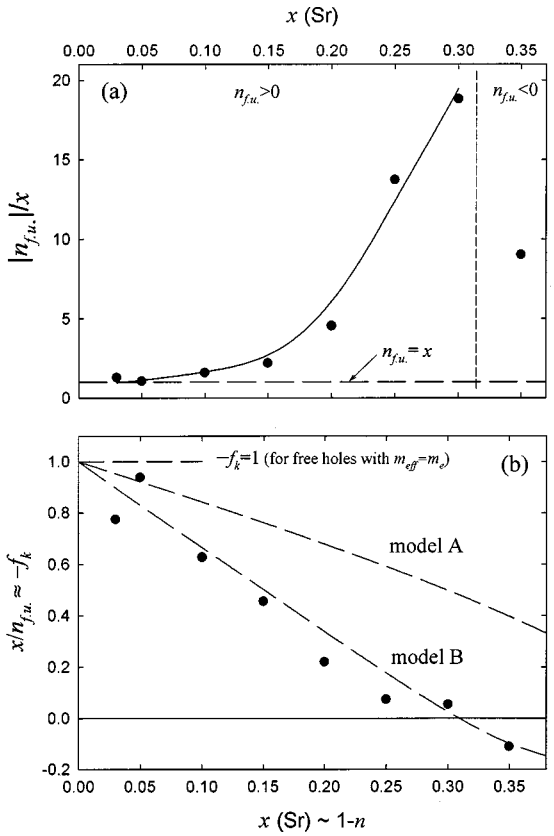


FIG. 6. (a) The ratio of the charge-carrier concentration per formula unit $n_{f.u.}$ (calculated from $R_H$) to the Sr concentration $x$; (b) experimental (points) and theoretical values (lines) of the freedom number $\hat{f}_k$ for a series of $La_{2-x}Sr_xCuO_4$ samples.

$$\hat{f}_k=\frac{n_{eff}}{n_H}\approx -\frac{x}{n_{f.u.}}. \tag{30}$$

In terms of this approach the change of the Hall coefficient sign in the function of Sr doping may be interpreted as a passage through the Fermi surface of zero-average curvature ($\hat{f}_k=0$) while the Fermi energy is changing. On the other hand, for low-Sr concentration the measured $\hat{f}_k\approx -1$, as for nearly-free holes with $|m_{eff}|\approx m_e$. This assumption is supported by recent ARPES experiments on $La_{2-x}Sr_xCuO_4$,[30] in which the inversion of the curvature of the Fermi surface was directly observed. The above picture may be described by a simple tight-binding model,

$$E(k_x,k_y)=-(\cos k_x+\cos k_y), \tag{31}$$

where $k_x$ and $k_y$ are normalized wave vectors. The above model will be called model *A*. The Fermi surfaces for this model are presented in Fig. 7(a). It is assumed that the band filling $n\approx(1-x)$, i.e., the completely filled band corresponds to $x=0$. The freedom number $\hat{f}_k$ calculated in the model *A* is presented in Fig. 6(b). However, the crossover from positive to negative values of $\hat{f}_k$ (i.e., change of the $R_H$ sign) occurs at $x=0.5$. Therefore, we have constructed a second, modified model in order to adjust the crossover point to the experimentally observed value $x\approx 0.32$. To be more realistic we have chosen the form of the correction term for the model *A* in such a way as to reproduce the ''squeeze'' of

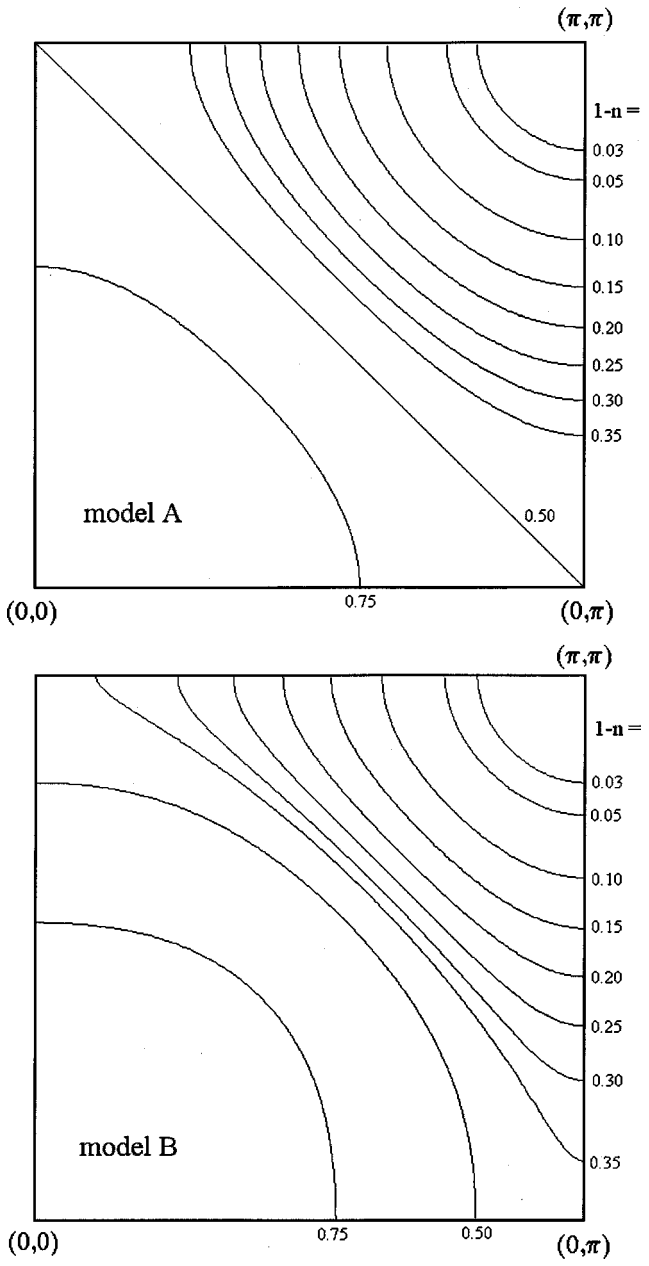


FIG. 7. The Fermi surfaces for the *A* and *B* models described in the text. The calculations have been performed for the band-filling values *n*, corresponding to the Sr concentration *x* in the investigated $La_{2-x}Sr_xCuO_4$ samples $(1-n=x)$, as well as for $1-n=0.5$ and 0.75.

the series of Fermi surfaces related to different *x* values along the diagonal of the Brillouin zone observed in ARPES experiments.[30] Finally, we have chosen the following form of the modified dispersion law:

$$E(k_x,k_y)=-(\cos k_x+\cos k_y)-0.17(\cos 2k_x+\cos 2k_y). \tag{32}$$

The modified model will be called model *B*. It should be treated as a result of matching of the initial model *A* to the experimentally determined *x* value, for which $R_H$ changes sign. The Fermi surfaces for this model are presented in Fig. 7(b), the freedom number $\hat{f}_k$ is shown in Fig. 6(b).

We have to emphasize that both models should be treated as only illustrative. The $LaCuO_4$ is frequently regarded as a charge-transfer insulator with a half-filled Hubbard band.[31,35] In this picture the Sr/La substitution introduces holes into the lower Hubbard band and makes the system metallic. Therefore, our phenomenological model may be regarded just as an effective model for the lower Hubbard band, in which the strong electron correlations making the $LaCuO_4$ insulating are effectively described by a single tight-binding band. We have proven that more realistic models, e.g., a simple one including only a second-nearest-neighbor hopping $[E(k)=-2t(\cos k_x+\cos k_y)-4t'\cos k_x\cos k_y$, Refs. 31 and 35] or more complicated models (e.g., Refs. 32,33,34), are not able to explain all compositional dependences of the transport coefficients.

Both models *A* and *B* were used for calculation of all measured quantities: $\sigma$, *S*, $R_H$, and $P_E$. The results are presented in Fig. 8. The electrical conductivity [Fig. 8(a)] was calculated using Eq. (23). The solid lines present the results of the simplified approach where $\sigma\sim n_{eff}$, not taking into account the dependence of the relaxation time $\tau$ on energy. However, for low-Sr concentration we could use a nearly-free-holes picture with $|m_{eff}|\approx m_e$. In this case we could use a high-temperature approximation $\tau(\epsilon)\sim\epsilon^{3/2}$ for the electron-phonon scattering, as in the formula (16). The results of the $\sigma\sim\tau n_{eff}$ calculations are presented as dashed lines. It can be seen that the results of both models generally reproduce the experimental data [see Fig. 5(a)]. However, for a more precise description a knowledge about the real $\tau(\epsilon)$ dependence would be necessary.

The thermoelectric power was calculated using Eq. (23) and the Mott-Jones formula

$$S=-\frac{\pi^2k_B^2T}{3|e|}\left(\frac{\partial\ln[\sigma_{xx}(\epsilon)]}{\partial\epsilon}\right)_{\epsilon=\zeta}, \tag{33}$$

where $k_B$ is the Boltzmann constant. The results are presented in Fig. 8(b). As for electrical conductivity, the solid lines present the results of the simplified approach where $\sigma\sim n_{eff}$, neglecting the energy dependence of the relaxation time. However, as shown by the dashed line (for model *B* only), taking into account the power-law dependence of $\tau(\epsilon)\sim\epsilon^{3/2}$ does not alter significantly the calculated $S(x)$ dependence. As we can see, both models *A* and *B* are able to reproduce the logarithmic dependence $S(x)$ observed experimentally for $x<0.20$ [see Fig. 5(b)]. Additionally, model *B* is also able to reproduce the minimum in the $S(x)$ dependence observed at $x\approx0.28$.

The Hall coefficient was calculated using formula (25) and the results are presented in Fig. 8(c). No correction for the relaxation time was necessary, since $R_H$ is independent of $\tau$ if it depends only on energy $[\tau=\tau(\epsilon)]$. Similar to the case of the thermoelectric power, both models *A* and *B* are able to reproduce the logarithmic dependence of $R_H$ on the Sr content observed for $x\lesssim0.30$ [see Fig. 5(c)]. However, model *B* is able also to explain the change in the Hall coefficient at $x\approx0.30$ [see the insets in Figs. 5(c) and 8(c)]. The mutual dependence between $R_H$ and *S* is shown in Fig. 9(b). As we can see, model *A* is able to reproduce only the linearity of the experimental dependence for $x\lesssim0.25$ [see Fig.

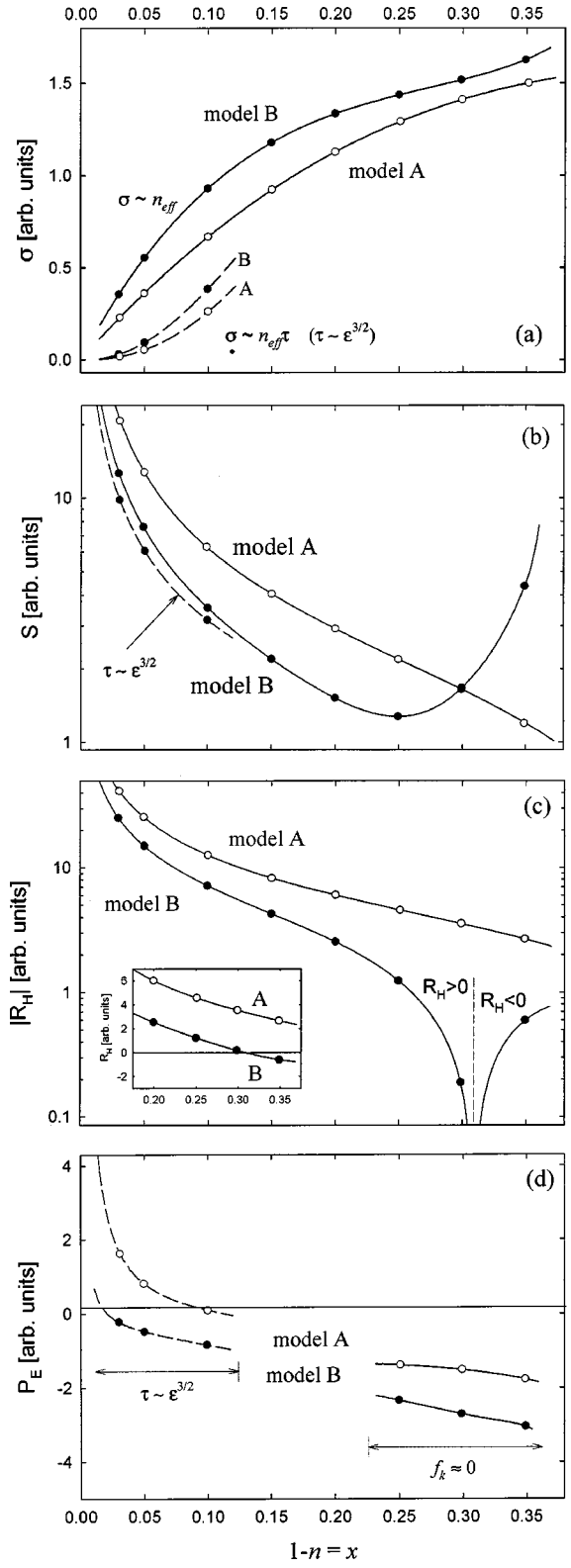


FIG. 8. Different transport coefficients for a series $La_{2-x}Sr_xCuO_4$ samples ($x=0.03-0.35$) calculated within *A* and *B* models: the electrical conductivity (a), the thermoelectric power (b), the Hall coefficient (c), and the Ettingshausen coefficient (d). The solid lines—no electron scattering taken into account; the dashed lines—a NFE, high-temperature approximation for elastic electron-phonon scattering, applicable only for low-Sr content. The inset in panel *c* shows, in the linear scale, the Hall coefficient in the vicinity of the Sr concentration, where $R_H$ evaluated in the model *B* changes sign.

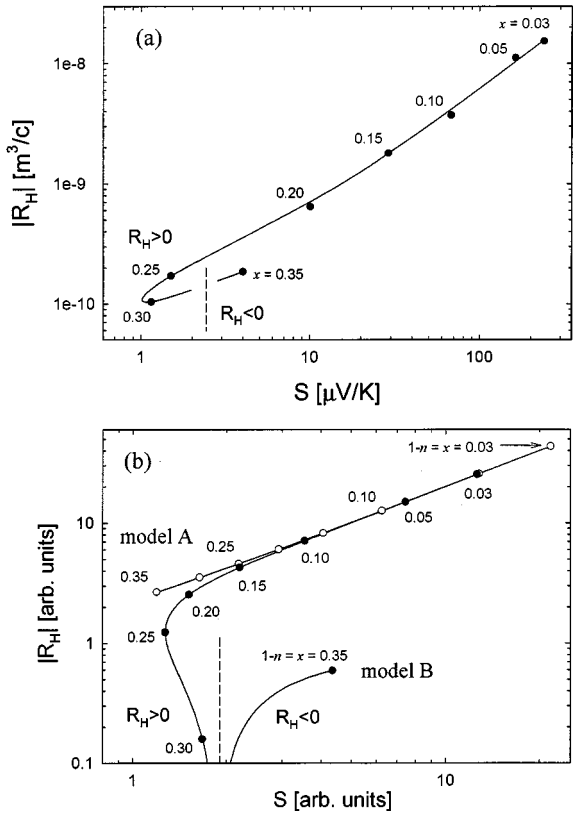


FIG. 9. The mutual dependence between the Hall coefficient and the thermopower: (a) experimental data, (b) calculated within the *A* and *B* models.

9(a)], whereas model *B* is able to qualitatively explain the U-turn observed in the experiment near $x=0.30$.

The Ettingshausen coefficient was calculated using Eq. (28). The results are shown in Fig. 8(d). The calculations have been performed in two approximations applicable for two Sr-content regions. For low-Sr concentration ($x\lesssim 0.10$) we have assumed the $\tau(\epsilon)\sim\epsilon^{3/2}$ dependence, as explained above. As shown by dashed lines, both models *A* and *B* are able to reproduce the observed change of $P_E$ sign from positive to negative for higher *x* values [see Fig. 5(d)]. This change is the result of a competition between the two mechanisms of the generation of the Ettingshausen effect in metals, which were described in Sec. II and illustrated by Figs. 1(c) and 1(d). For lower *x* values the transversal temperature gradient is caused mainly by the dependence of the relaxation time $\tau$ on the charge carriers energy [the ''scattering'' mechanism described by the first term in Eq. (28), see Fig. 1(c)], which gives a positive Ettingshausen coefficient [compare formula (16) for nearly-free charge carriers in the high-temperature limit, which foresees positive $P_E$ for holes]. For higher *x* values the second mechanism is prevailing. Here the transversal temperature gradient is caused mainly by the fact that electrons of different energy are moving along isoenergetic surfaces of different average curvature [the ''curvature'' mechanism, see second term in the Eq. (28) and Fig. 1(d)].

In the region of high-Sr concentration ($x\gtrsim 0.25$) we could assume that $\hat{f}_k\approx 0$ and neglect the first term from formula (28). Thus, in this region the Ettingshausen effect is only caused due to the dependence of average Fermi surface cur-

vature on the charge-carriers energy (the ''curvature'' mechanism). In this manner, both models *A* and *B* (see solid lines) are able to explain the experimentally observed negative and weakly variable values of the Ettingshausen coefficient for high-Sr concentration.

Two remarks have to be given concerning the region of low Sr concentration. As emphasized in Sec. IV, the Ettingshausen effect generated by the metallic mechanisms [Eq. (17)] may be sufficiently depressed if the phonon thermal conductivity is comparable to the thermal conductivity due to electrons. This true for the case of $La_{2-x}Sr_xCuO_4$, therefore it seems to be impossible to experimentally observe very large values of the Ettingshausen coefficient, which might be predicted by Eqs. (28) or (16) ($P_E \rightarrow \infty$ if $E_F \rightarrow 0$, i.e., $P_E \rightarrow \infty$ if $x \rightarrow 0$). The second remark concerns the fact that $P_E$ values are positive for very low-Sr concentration. In this range the $La_{2-x}Sr_xCuO_4$ undergoes a transformation to the charge-transfer insulator for $x \rightarrow 0$. Thus, in the vicinity of this transformation the ''semiconductor'' mechanism of the Ettingshausen effect generation [see Eq. (9) and Fig. 1(b)], which results in large, positive $P_E$ values, cannot be here ruled out. This approach may be used as a concurrent explanation of the positive sign of the observed Ettingshausen coefficients for low $x$ values if the assumption of $\tau(\epsilon) \sim \epsilon^{3/2}$ is not appropriate.

## VI. SUMMARY

The room-temperature values of the electrical conductivity $\sigma$, the thermoelectric power $S$, the Hall coefficient $R_H$, and the Ettingshausen coefficient $P_E$ have been measured for a series of $La_{2-x}Sr_xCuO_4$ samples ($x=0.03$–$0.35$). It was observed that with increasing Sr content $x$: (i) $\sigma$ increases monotonically by one order of magnitude over the whole composition range; (ii) $S$ decreases logarithmically by two orders of magnitude down to $x=0.25$, then a wide minimum was observed near $x=0.28$, $S$ remains positive for all compositions; (iii) $R_H$ is positive and decreases logarithmically by two orders of magnitude down to $x=0.32$, then $R_H$ changes sign into negative; an almost linear relation between $S$ and $R_H$ was observed for all compositions with an exception of $x=0.35$, for which $S$ and $R_H$ are of opposite signs; (iv) $P_E$ is of the order of magnitude characteristic for metals for all compositions; $P_E$ is positive for low-Sr concentration ($x=0.03$ and $0.05$) and negative for all other compositions.

To analyze the behavior of all measured transport coefficients, a simple, tight-binding-like model was constructed. The model effectively describes the crossover from the charge-transfer insulator ($LaCuO_4$) to the metal while substituting the $La^{+3}$ by $Sr^{+2}$ ions. An evolution of the average curvature of the Fermi surface from positive to negative values is also described by the model. It has been indicated that the nearly-free-electrons picture may used only for low-Sr concentration ($x \lesssim 0.10$). The conclusions may be summarized as follows: (i) $\sigma$ grows and $S$ and $R_H$ fall down with increasing Sr content $x$ mainly due to the increase of the effective electron concentration $n_{eff}$; (ii) $R_H$ changes sign and $S$ exhibits a minimum near $x \approx 0.3$ because of the sign change of the average curvature of the Fermi surface; (iii) for high Sr concentration $P_E$ is negative due to the domination of the ''curvature'' mechanism (carriers of different energies move along isoenergetic surfaces of different curvatures); (iv) for low-Sr concentration the ''scattering'' mechanism is dominating, what results in the positive $P_E$ sign (carriers of different energies move along holelike isoenergetic surfaces of the same curvature, but the higher-energy carriers are stronger scattered).

## ACKNOWLEDGMENTS

The authors would like to acknowledge the valuable discussions with P. Wróbel. We would like also to thank C. Sułkowski for the thermopower measurements. The work was supported by the Polish State Committee for Scientific Research under Contract No. 2PO3B 11613.

[1] S.D. Obertelli, J.R. Cooper, and J.L. Tallon, Phys. Rev. B **46**, 14 928 (1992).
[2] See, e.g., S. Martin, A.T. Fiory, R.M. Fleming, L.F. Schneemeyer, and J.V. Waszczak, Phys. Rev. B **41**, 846 (1990).
[3] Y. Kubo and T. Manako, Physica C **197**, 178 (1992).
[4] F. Devaux, A. Manthiram, and J.B. Goodenough, Phys. Rev. B **41**, 8723 (1990).
[5] H. Takagi, T. Ido, S. Ishibashi, M. Uota, S. Uchida, and Y. Tokura, Phys. Rev. B **40**, 2254 (1989).
[6] S. Uchida, H. Takagi, and Y. Tokura, Physica C **163-164**, 1677 (1989).
[7] P.W. Bridgman, Phys. Rev. **24**, 644 (1924).
[8] H. Fieber, A. Nedoluha, and K.M. Koch, Z. Phys. **131**, 143 (1952).
[9] B.V. Paranjape and J.S. Levinger, Phys. Rev. **120**, 437 (1960).
[10] H. Mette, W.W. Gärtner, and C. Loscoe, Phys. Rev. **115**, 537 (1959).
[11] H. Mette, W.W. Gärtner, and C. Loscoe, Phys. Rev. **117**, 1491 (1960).
[12] E.H. Putley, Proc. Phys. Soc. London, Sect. B **68**, 35 (1955).
[13] F.J. Blatt, *Physics of Electronic Conduction in Solids* (McGraw-Hill, New York, 1968).
[14] A.A. Abrikosov, *Fundamental of the Theory of Metals* (North-Holland, Amsterdam, 1988).
[15] E.H. Sondheimer, Proc. R. Soc. London, Ser. A **193**, 484 (1948).
[16] *International Critical Tables* (McGraw-Hill, New York, 1929), Vol. 6, p. 419.
[17] L. Zecchina, Phys. Status Solidi **42**, K153 (1970).
[18] See, e.g., G.E.R. Schulze, *Metallphysik* (Springer-Verlag, Berlin, 1974).
[19] C.M. Hurd, *The Hall Effect in Metals and Alloys* (Plenum, New York, 1972).
[20] T. Plackowski and M. Matusiak, Supercond. Sci. Technol. **12**, 610 (1999).
[21] C. Sułkowski, T. Plackowski, and W. Sadowski, Phys. Rev. B **57**, 1231 (1998).
[22] B.M. Anderson and B. Sundqvist, Phys. Rev. B **48**, 3575 (1993).
[23] M. Ikebe, H. Fujishiro, K. Nakasato, and K. Noto, Physica C **263**, 309 (1996).

[24] R.C. Yu, M.B. Salomon, J.P. Lu, and W.C. Lee, Phys. Rev. Lett. **69**, 1431 (1992).
[25] P.B. Allen, X. Du, L. Mihaly, and L. Forro, Phys. Rev. B **49**, 9073 (1994).
[26] M. Matsukawa, K. Iwasaki, K. Noto, Y. Yamada, and S. Horii, Jpn. J. Appl. Phys. **36**, 4414 (1997).
[27] D.T. Morelli, G.L. Doll, J. Heremans, M.S. Dresselhaus, A. Cassanho, D.R. Gabbe, and H.P. Jenssen, Phys. Rev. B **41**, 2520 (1990).
[28] M. Sera, S. Shamoto, M. Sato, I. Watanabe, S. Nakashima, and K. Kumagai, Solid State Commun. **74**, 951 (1990).
[29] M. Suzuki, Phys. Rev. B **39**, 2312 (1989).
[30] A. Ino, C. Kim, T. Mizokawa, Z.-X. Shen, A. Fujimori, M. Takaba, H. Eisaki, and S. Uchida, http://xxx.lanl.gov/abs/cond-mat/9809311 (unpublished); A. Fujimori, A. Ino, T. Mizokawa, C. Kim, Z.-X. Shen, T. Sasagawa, T. Kimura, K. Kishio, M. Takaba, K. Tamasaku, H. Eisaki, and S. Uchida, J. Phys. Chem. Solids **59**, 1892 (1998).
[31] R. Micnas and S. Robaszkiewicz, in *High-$T_c$ Superconductivity 1996: Ten Years after the Discovery*, edited by E. Kaldis, E. Liarokapis, and K.A. Müller (Kluwer Academic, Dordrecht, 1997), p. 31.
[32] J. Ruvalds and A. Virosztek, Phys. Rev. B **42**, 399 (1990).
[33] H. Ushio, T. Schimizu, and H. Kamimura, J. Phys. Soc. Jpn. **60**, 1445 (1991).
[34] R. Hopfengärtner, M. Leghissa, G. Kreiselmeyer, B. Holzapfel, P. Schmitt, and G. Saemann-Ischenko, Phys. Rev. B **47**, 5992 (1993).
[35] R.S. Markiewicz, J. Phys. Chem. Solids **58**, 1179 (1997).